ELSEVIER

Journal of Nuclear Materials 306 (2002) 153–172

journal of nuclear materials

www.elsevier.com/locate/jnucmat

Microstructure of irradiated SBR MOX fuel and its relationship to fission gas release

S.B. Fisher [a,*], R.J. White [a], P.M.A. Cook [a], S. Bremier [b], R.C. Corcoran [c], R. Stratton [d], C.T. Walker [b], P.K. Ivison [e], I.D. Palmer [f]

[a] *British Nuclear Fuels plc, Sellafield, Seascale, Cumbria, CA20 1PF, UK*
[b] *European Commission, Joint Research Centre, Institute for Transuranium Elements, Postfach 2340, D-76125, Karlsruhe, Germany*
[c] *BNFL R&T, Nuclear Generation, Berkeley Centre, Berkeley, Gloucestershire, GL13 9PB, UK*
[d] *Nordostschweizerische Kraftwerke, Parkstrasse 23, Baden CH-5401, Switzerland*
[e] *AEA Technology, Windscale, Seascale, Cumbria, CA20 1PF, UK*
[f] *British Nuclear Fuels plc, Springfields, Preston, Lancashire, PR4 OXJ, UK*

Received 28 January 2002; accepted 14 September 2002

Abstract

SEM and EPMA examinations of the microstructure and microchemistry of British Nuclear Fuel's quasi-homogeneous SBR MOX fuel following irradiation suggests behaviour which is very similar to that observed in UO_2. Most significantly, a fission gas release of 1% in three-cycle SBR MOX PWR rods is associated with the development of a well-defined intergranular bubble network, which has not been seen previously in the more heterogeneous MOX fuels irradiated under similar conditions. The contrast between the observations is attributed to the relatively low volume fraction and small size of the Pu rich inhomogeneities in the SBR fuel which generate only 4% of the total fission gas and eject most of this into the surrounding mixed oxide matrix. The resulting perturbation in the Xe distribution has a negligible influence on the evolution of the microstructure. A key observation is made from the results of recent post-irradiation annealing experiments performed on SBR MOX and UO_2. These confirm near identical fission gas behaviour in the two fuel types when the influence of thermal conductivity and rod rating are removed.

1. Introduction

This is the final paper in a series [1–6] describing the results of the first commercial irradiation of British Nuclear Fuel's SBR MOX fuel that took place over the period 1994–1997 in assembly M501 of the Beznau-1 PWR, Switzerland. Seven pre-characterised rods with burnups in the range 31–35 MWd/kgHM were taken for post-irradiation examination (PIE) at the European Institute for Transuranium Elements (ITU). In a previous publication [5] the fission gas release data obtained from the M501 rods were compared with those from UO_2 and other MOX fuels. It was shown through calculations using the Enigma fuel performance code [7] that the behaviour of SBR MOX was very similar to that of UO_2 when allowance was made for its lower thermal conductivity and higher third cycle rating. Specifically, it was shown that the temperature threshold for gas release in the material, when irradiated under normal PWR conditions, is similar to that for UO_2 fuel, implying that the mechanisms of release and the microstructure parameters that define them are also similar. In this paper the comparison of UO_2 and SBR MOX is taken a stage further through a detailed electron probe microanalysis (EPMA) study of the microstructure and microchemistry of the irradiated SBR MOX. The results, which track the xenon production and dispersal in this material, account for its UO_2 – like behaviour.

* Corresponding author. Tel.: +44-1726 810825.
E-mail address: stanfisher@onetel.net.uk (S.B. Fisher).

0022-3115/02/$ - see front matter
PII: S0022-3115(02)01247-3

To place this new work in context a review of related studies is first presented. Methods of fabrication, resultant fuel microstructures, and the irradiation conditions are described for M501 and other MOX fuels. The fission gas release mechanism for UO_2 is then re-examined to identify the key microstructural parameters for comparison in MOX fuels. Most importantly, the pioneering EPMA studies performed at ITU on optimised co-milled (OCOM) MOX are described and the results compared with similar work on the micronised master mix (MIMAS) fuel. The techniques applied in the SBR MOX investigations were derived from this previous work but it will be seen that they provide a very different description of behaviour in this quasi-homogeneous material.

2. MOX fabrication routes and resultant microstructures

A detailed comparison of as-fabricated microstructures of MOX fuels was given in the paper dealing with fission gas release [5]. Here it is sufficient to list the manufacturing processes and tabulate the key features of the resultant microstructures.

MIMAS fuel is produced at facilities in Dessel (Belgonucleaire), Cadarache (COGEMA) and MELOX (COGEMA) [8–10]. MOX OCOM is a similar fuel that was made by Siemens-KWU and has been irradiated in reload quantities in a number of German commercial reactors [11]. Both fabrication routes involved the blending of a master mix rich in PuO_2 with UO_2 powder (prepared using the AUC or ADU routes) and scrap from MOX pellet production. Both fuels consist of Pu rich spots in a $(UO_2 + PuO_2)$ matrix which may, exceptionally, reach sizes of $\simeq$150 and 200 μm, respectively [9,12], with a Pu concentration not exceeding that in the primary blend.

A limited amount of MOX fuel was made at Cadarache by COGEMA using the COCA (cobroyé-Cadarache) process before it was abandoned [9]. This involved direct co-milling of the oxides and produced a fuel with a relatively homogeneous microstructure. Although there is only limited PIE data on this fuel there are some reports of its irradiated microstructure in relation to fission gas release that are obviously significant in the context of this paper and these will be referred to in later sections.

In the manufacture of SBR MOX, PuO_2 and IDR-UO_2 (Integrated Dry Route) powders and, if necessary, crushed and milled scraps, are mixed directly in an attritor mill. The feed powders are added in the proportions of the final enrichment and are milled for a limited time. This method of manufacture produces fuel in which the plutonium is quasi-homogeneously distributed. The area fraction of the fuel with a plutonium concentration of higher than 20 wt% is 1–2%, depending on the initial Pu content. The cut-off for defining a Pu spot was taken to be 20 wt% Pu, since this was the threshold concentration used in the characterisation of as-fabricated material [13]. If the cut-off is lowered from 20 to 15 wt% the calculated area fraction of plutonium spots in the M501 fuel increases from 1% to around 5%. The largest of the Pu rich spots in SBR fuel are 30–35 μm in diameter with a Pu concentration averaged across the spot of 25–35 wt%, although the peak Pu concentration in the spot may reach 60 wt%. The M501 fuel described in this paper was produced in the MOX Demonstration Facility (MDF) at Sellafield.

Table 1
Area fractions of phases and distribution of input plutonium in the MOX fuels referred to in the paper

	MIMAS AUC	OCOM 15	OCOM 30	SBR
Area fraction of phases (%)				
Matrix	75.4	66	83	98–99
Pu rich spots	24.6	34	17	1–2[a]
Distribution of input Pu (%)				
Matrix	39	3	3.5	96
Pu rich spots	61	97	96.5	4

[a] Discrete areas containing more than 20 wt% Pu.

The microstructures of the SBR and MIMAS fuels were compared in [5]. Table 1 summarises the proportions of each phase present in the microstructures and the distribution of plutonium prior to irradiation.

3. Irradiation conditions

Throughout this paper reference is made to irradiation data and microstructural observations on PWR irradiated UO_2, MIMAS AUC and OCOM fuels that come almost exclusively from Refs. [9,10,12]. Table 2 draws together the main characteristics and irradiation conditions for these MOX fuels and compares them with corresponding data for the highest power SBR MOX fuel rod from M501, rod 4567. EPMA results on transverse sections from this rod are the focus of this paper. Table 3 describes the location, burnup, rating and irradiation temperature of the sections analysed.

4. Comparison of fission gas behaviour in UO_2 and MOX fuel

Under thermal irradiation conditions the yield of the long-lived fission gas isotopes of Xe and Kr generated from ^{235}U and ^{239}Pu is about 28 atoms and 31 per 100 fissions [5]. If a significant fraction of the gas is released

Table 2
Fuel pellet and fuel rod design characteristics and irradiation data for the MOX fuels referred to in the paper

	MIMAS AUC	OCOM 15	OCOM 30	SBR MOX (rod 4567)
Fuel density (%TD)	95	95	95	95
Grain size (μm)	5–10	5–6	5–6	7.8
Pu content (wt%HM)	2.9–6.7	5.03	5.07	5.54
$^{235}U/^{238}U$ (%)	Depleted	0.72	0.72	0.3
Pu rich spots (vol.%)	24.6	34	17	1
Average Pu content of spots (wt%)	12.5	13.2	26.5	25–35
Maximum size of Pu rich spots (μm)	~150	~200	~200	30–35
Stoichiometry (O/M)	~2.00[a]	1.994	1.992	2.00
Pellet diameter (mm)	Various	9.13	9.13	9.29
He fill gas pressure (bar)	25	22.5	22.5	20
Cladding material	Zircaloy 4	Zircaloy 4	Zircaloy 4	Zircaloy 4
Nominal fuel-clad gap width (μm)	85	85	85	100
Maximum fuel temperature (°C)	1200[b]	<1300	<1300	1130[c]
Rod burn-up (MWd/kgHM)	9–52	43.6[d]	44.5[d]	35.6
Cycles/rod average power ($kW\,m^{-1}$)	4/21	4/19.4[e]	4/20.4[e]	3/20

[a] Close to stoichiometric [9].
[b] Meteor calculations [9].
[c] Calculated using the Enigma code [7].
[d] Irradiated as rod segments, burnups given are for the segments studied by EPMA.
[e] For the particular fuel segments studied by EPMA.

Table 3
Transverse sections cut from rod 4567 for EPMA

Section	Axial location[a] (mm)	Time-averaged rating (kW/m)	Average burnup[b] (MWd/kgHM)	Peak centre temperature[b] (°C)
CT10	601	21.9	38.7	1126
CT11	1721	22.2	38.9	1068
CT12	2588	19.0	33.6	946
CT20	2250	21.9	38.6	1051

[a] Distance from bottom of rod.
[b] Calculated using the Enigma code [7].

to the rod free volume it can adversely affect thermal performance at even moderate burnup; at high exposures it could lead to rod overpressure. If the gas is retained in the fuel it can cause high swelling. Consequently, fission gas release has been the subject of intensive study since the early 1960s. Over the past five years new electron microscopic evidence from well-planned experiments has consolidated a mechanistic model developed in the early nineties which is now generally accepted as a satisfactory description of fission gas behaviour in UO_2 [14–17].

4.1. Fractional release

The M501 rod releases are compared with corresponding data [9] from MIMAS AUC, MOX COCA, MIMAS ADU and IDR-UO_2 in Fig. 1. Also in the figure are results from the OCOM fuel segments whose EPMA [12] is one of the key points of reference here. EPMA was performed on fuel sections from segments with burnups of 43.6 MWd/kgHM (OCOM 15) and 44.5 MWd/kgHM (OCOM 30), see Table 2. Note that only those rods experiencing broadly similar power histories are included in Fig. 1. Fission gas data from AUC-UO_2 fuel irradiated in Germany are not included due to high beginning of life powers that result from different operating strategies. The figure shows that MOX fuels in general have significantly higher final gas release than the UO_2 data shown and that there is apparently little to separate the behaviour of the different types of MOX fuel. Much of this enhancement in gas release can be explained by the reduced thermal conductivity and higher end of life ratings in MOX compared with UO_2, that results in higher end-of-life centre temperature [5]. If the higher operating temperature is the sole or overriding cause of the enhanced release in MOX fuel, it follows that the mechanism of release is similar to that in UO_2 and also that the fission gas diffusion coefficients, generation rates, and all the microstructural parameters controlling release are similar. Whilst it is conceivable that the quasi-homogeneous SBR MOX could respond to irradiation in a similar way to UO_2, it is more difficult to envisage for the more heterogeneous fuels MIMAS AUC or OCOM. Indeed, as will be shown later, EPMA studies on these MOX variants, irradiated under normal PWR conditions, found no evidence for the development of an intergranular bubble network

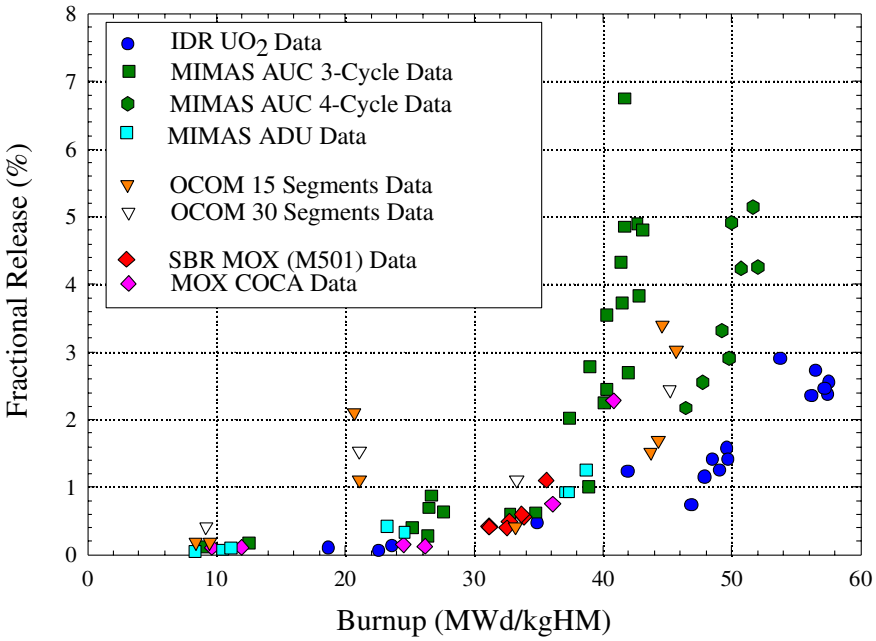

Fig. 1. Measured fractional fission gas releases from MIMAS AUC, MIMAS ADU, MOX COCA and IDR UO_2 rods [9], compared with those from SBR MOX rods irradiated in the M501 programme. Some data from irradiated OCOM segments are also included because reference is made to the microstructural studies performed on them [12].

despite releases of up to 5% and 3.5%, respectively [9,12].

4.2. Fission gas generation rate

Despite the marked differences in the fissile composition of MOX and UO_2 fuels, the fission gas generation rates are similar. In [5] the fission gas generation rate for rod 4567 was determined using the physics code, CASMO [18] to obtain the through life fission mix. This was found to be 65.8% ^{239}Pu (thermal), 23.2% ^{241}Pu (thermal), 2.2% ^{235}U (thermal), with the remainder being ^{238}U fast fissions. Using these values a gas generation rate of 27.19 ml (at STP) per MWd was obtained. This compares with a generation rate of 28.08 ml per MWd for an extreme fission mix of 90% ^{235}U (thermal) and 10% ^{238}U (fast). Thus, for the purposes of this paper the fission gas generation rates of MOX and UO_2 fuel can be assumed to be the same. Moreover, in both fuel types substantially more Xe than Kr is generated. In rod 4567, Xe constituted 94% of the fission gases generated. In analyses of fission gas behaviour it is therefore sufficient to track the Xe and assume Kr follows the same path.

4.3. Fission gas diffusion coefficients

Turnbull derived values for the diffusion coefficients of the Xe and Kr isotopes in UO_2 over the temperature range 250–1400 °C [19]. The composite coefficient obtained has three terms: lattice diffusion at high temperatures, lattice assisted by irradiation-produced vacancies at intermediate temperatures (700–1200 °C), and an athermal (irradiation) component at low temperatures. It is likely that the presence of an irradiation component, even at PWR rod centre temperatures, makes the coefficient less sensitive to fuel composition.

No analysis corresponding to the above exists for MOX fuels and so a comparison must be attempted indirectly. In this respect, the two most useful pieces of evidence for SBR MOX are the general agreement of the release of the stable gases in the M501 rods with the UO_2 based Halden criterion [5] and the comparison of the Halden rig IFA-633 unstable fission product release data for the two fuels. In the latter, analysis of the fuel surface-to-volume ratio as a function of measured fuel centre temperature yielded very similar curves for UO_2 and SBR MOX when the gas diffusion coefficients were assumed to be the same [20]. In both these instances it is the rod-averaged diffusion coefficient that is tested since the release was from the rod as a whole.

5. Comparison of microstructure parameters affecting gas release in SBR MOX and UO_2 fuel

5.1. Grain size

The grain size of oxide fuels is an important parameter in any model of diffusional gas release. This

follows directly from Booth's [21] original calculation of gas diffusion to grain boundaries, which gave a release inversely proportional to grain size. This mechanism remains fundamental to most current fuel performance models. In such models the requirement for polycrystalline fuels to develop a network of grain boundary tunnels before rapid release can occur results in the virtual elimination of a grain size dependence at low levels of release as the effects of grain boundary area compensate for grain size. The Enigma code [7,17] predicts little grain size dependence for releases near the Halden threshold of 1%, and this is confirmed in irradiation tests (see e.g. Ref. [22]).

The MLI (mean linear intercept) grain size prior to irradiation of the fuel used in M501 rod 4567 was 7.8 μm. Post-irradiation measurements [3] on this fuel suggest that there was grain growth of 1–2 μm in the central region in agreement with Enigma predictions. A grain size of 8–10 μm would therefore have existed in the centre of rod 4567 for most of the relevant period of exposure.

The grain size of UO_2 fuel is generally $\simeq$10 μm [23,24] and little grain growth occurs under normal operating conditions. Thus, during the critical phases of fission gas diffusion to boundaries and its accumulation into an intergranular bubble network up to the point of 1% release the grain size in the central region of the M501 fuel was of the order of that in most standard UO_2 fuels. The small difference would have had a negligible influence on release at the low levels under consideration here.

5.2. Fuel pellet cracking

The extent of pellet cracking during fuel operation has an obvious influence on fission gas release since it creates free surface to which gases may diffuse (or otherwise be transported by recoil or knock-out) and thereby be released into the rod free volume.

Recent pellet fragmentation measurements made on M501 rods are consistent with UK data from UO_2 fuel irradiated with similar power histories [3].

5.3. As-fabricated porosity

SBR MOX has generally been manufactured to a target geometric density of 95% theoretical or 10.45 g/cm^3. Stability is achieved through the use of a pore former, CONPOR, and the resulting as-fabricated porosity distribution is a classic bimodal with peaks at $\simeq$1 and 10–20 μm [6]. Total porosity is $\simeq$4.5% of which a quarter is contributed by the lower peak of intrinsic porosity. Very similar porosity distributions are obtained in IDR based UO_2 fuels that are also prepared with a pore former [25].

Although the porosity distributions in SBR MOX and IDR-UO_2 are generally similar, fuel densification data from the BNFL Halden experiment IFA-633 has shown that the MOX fuel densifies significantly more in the early stages of irradiation and this is attributed [6] to the initially smaller grain size providing a higher sink density for vacancies. Relative to UO_2, then, the remaining porosity in SBR MOX will offer a lower matrix sink for fission gases.

5.4. Intragranular bubbles and dislocation density

Transmission electron microscopy (TEM) of irradiated UO_2 [15,26] has shown that the matrix contains a large population, $\simeq 10^{24}$ m^{-3}, of small nanometre-size cavities. These quickly attain their final density and size, which appear to be largely independent of burnup. The cavities are often observed to lie in straight lines and Turnbull [27] proposed that they were nucleated in the wake of fission fragments. These cavities grow by the capture of gas atoms and are destroyed by fission fragments which return the gas to solution; a steady-state morphology results.

Though no TEM of M501 fuel has been undertaken, SBR MOX from the Callisto experiment [28] has recently been comprehensively examined by TEM and scanning electron microscopy (SEM). The microstructures observed in the irradiated MOX were very similar to those seen previously in UO_2 fuel. Table 4 details the data obtained for intragranular cavities and dislocations in the Callisto fuel and compares them with the corresponding data for IDR-UO_2 from [15].

It is useful to estimate the relative strengths [29] of the various sinks for gas atoms that are present in the microstructures of the two fuels. For the intrinsic porosity this strength is $\simeq 3 \times 10^9$ m^{-2}, for dislocations $\simeq 4 \times 10^{13}$ m^{-2} and for boundaries $\simeq 4 \times 10^{11}$ m^{-2}. In contrast the figure for the intragranular cavities is overwhelming at $\simeq 10^{15}$ m^{-2}. Accordingly, the most likely route for gas atoms to reach the boundaries following creation within the matrix is absorption/ejection at intragranular cavities until random diffusion takes them to a boundary and into a bubble. Even then the atoms may be returned to the grains by irradiation-induced re-solution [17].

5.5. Intergranular bubbles

Studies on Advanced Gas Reactor (AGR) fuel have now comprehensively itemised the statistics of intergranular bubble nucleation and growth, coalescence, and grain edge interlinkage for UO_2 fuel [15,17]. An example of grain face porosity in post-irradiated annealed AGR UO_2 is shown in Fig. 2(a). It is seen that the morphology of the porosity can vary widely from face to face even on the same grain. Variations of a factor ten in

Table 4
Data on intragranular bubbles and dislocations in UO_2 and SBR MOX obtained from TEM measurements

Fuel type	Burn-up (MWd/kgHM)	Sample temperature (°C)	Intergranular cavities		Dislocation density (m^{-2})
			Density (m^{-3})	Radius (nm)	
UO_2[a]	Various	800–1000	2.0×10^{24}	$0.5 - 1.0$	$2.7 \pm 1.0 \times 10^{13}$
SBR MOX[b]	27.1	~1400	1.7×10^{24}	0.6	$5.2 \pm 2.5 \times 10^{13}$

[a] From Ref. [15].
[b] Recent measurements made on fuel irradiated in the Callisto experiment [28].

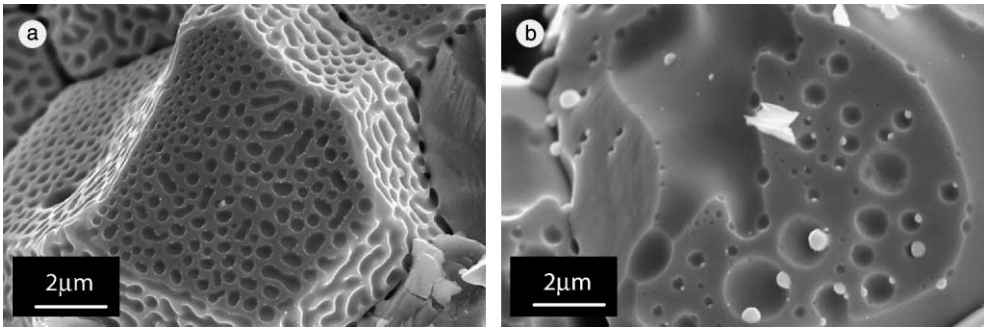

Fig. 2. Intergranular bubbles on grain faces in (a) UO_2 and (b) SBR MOX. The MOX fuel was irradiated as short rods in the Callisto experiment [28] at temperatures up to 1400 °C to a burnup of 27.1 MWd/kgHM and showed a gas release of ~4%. The UO_2 example is from the 'library' of images collected in the study of AGR fuel [16,17] and illustrates the variation in bubble development from face to face on one grain. Both images also show evidence of 'five metal' precipitates associated with the bubbles.

bubble density and two in swelling and fractional coverage are commonplace, and probably arise from the effects of neighbouring grain orientation, or size [17].

It has been reported [9] that PWR-irradiated UO_2 displays intergranular bubbles when gas release to the rod free volume reaches 2–3%, which is obtained at a burn-up of around 55 MWd/kgHM (see Fig. 1). In contrast, no such features have been seen in MIMAS AUC [9] and OCOM [12] fuels irradiated under normal operating conditions even though releases of 4–5% and ≃3.5% were measured. However, after irradiations where power increases occurred and corresponding high temperatures were attained, complete networks have been seen in MIMAS AUC [9], as in the Callisto SBR MOX which had experienced temperatures of up to 1400 °C in BR2, Fig. 2(b). In contrast, networks of grain boundary fission gas bubbles have been observed in the M501 fuel irradiated under normal PWR operating conditions and showing a release of 1.1%.

5.6. Distribution of the fissile isotope

In UO_2, the fissile isotope ^{235}U is homogeneously distributed throughout the fuel, whereas in MOX fuel part of the fissile isotope ^{239}Pu is concentrated in spots. Consequently, in MOX fuel fission gas generation and release is not the same at all points in the material.

Several papers over the past two years [3,4,13] have described the development of quantitative techniques for the characterisation of the plutonium distribution in unirradiated SBR MOX using energy dispersive X-ray mapping. They have shown that the fuel is primarily an homogeneous mix of UO_2 and PuO_2 in which regions of relatively high Pu content are dispersed as small ≃10 μm spots in the matrix. It has also been demonstrated in M501 fuel, through the use of wavelength dispersive X-ray analysis, that irradiation had little effect on the distribution of Pu spot size or volume fraction, except that the volume fraction of spots diminishes. Almost 70% of Pu spots are ≃10 μm or less in diameter, both before and after irradiation [3,4].

6. Review of EPMA post-irradiation results for OCOM, MIMAS AUC and COCA MOX fuel

At burnups in the range 43–55 MWd/kgHM the Pu spots in both OCOM and MIMAS AUC fuel become highly porous. The fission gas bubble size within them varies with radial position; in spots towards the cooler outside of the pellet they are generally smaller than in the central region where there are often just a few large pores, Fig. 3. Exceptions to this rule may occur very close to the pellet rim where the burnup rises steeply [12].

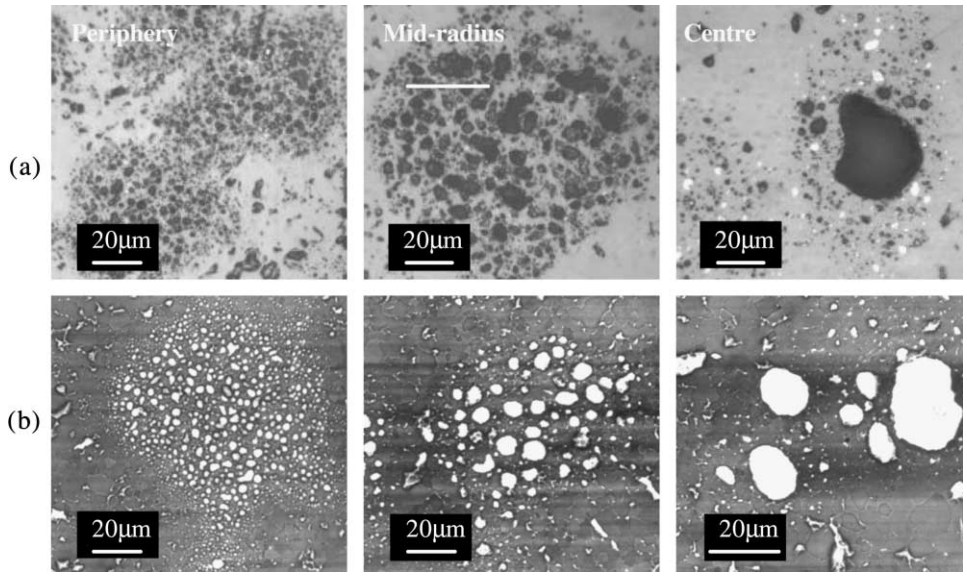

Fig. 3. Across pellet appearance of Pu rich spots in irradiated (a) MIMAS AUC and (b) OCOM 30. The former are optical micrographs and the latter electron absorption micrographs. The burnups of the two MOX fuels are 55 and 44.5 MWd/kgHM, respectively. Even in the central regions most of the Xe generated remains in large pores within the spots.

The burnup in the spots, calculated from the local Nd concentration, reached ≃150 MWd/kgHM at an average pellet burnup of 45 MWd/kgHM in MIMAS AUC, and 110 or 190 MWd/kgHM at the pellet centres of the OCOM 15 and 30 samples, respectively [12].

In MIMAS AUC irradiated to an average burnup of 55 MWd/kgHM the overall generated Xe concentration was ≃0.77 wt%. However, its morphology as micron-sized gas bubbles in the large Pu rich spots gave rise to local measurements as low as 0.1–0.3 wt%. Although its form in the UO_2 matrix allowed more effective measurement, the low fissile content here combined with the measurements in the spots resulted in a pellet average of only 0.4 wt%. Fig. 4(a) summarises these data taken from [9], showing the approximate range of the Xe measurements over the pellet radius and the disparity between these and the calculated Xe generation. Similar behaviour was seen in the OCOM material. Xe measurements in the Pu rich spots of OCOM 30 were ≃0.25 wt%, with an integrated average across the pellet of 0.52 wt%, compared to an estimated 0.63 wt% generated for a burnup of 44.5 MWd/kgHM using the same conversion factor as for MIMAS AUC above. Fig. 4(b) shows the radial Xe distribution in the UO_2 matrix. Given the reported Nd levels [12], the Xe concentration in the OCOM MOX matrix would be expected to exhibit a similar range to that observed in the MIMAS AUC. In both these fuels, then, the Xe created in the spots accumulates into pores and is not measured effectively and the surrounding UO_2 matrix is relatively low in Pu compared to, say, the matrix of homogeneous material. In neither of the fuels, irradiated under normal PWR operating conditions, are intergranular bubble networks observed.

The performance of the more homogeneous MOX COCA in respect of Xe measurement was discussed briefly in [9] and it provides an interesting contrast to the behaviour above. The pellet examined was from a rod with a burnup of 46 MWd/kgHM showing a release of 2.3%. In this instance the estimated overall Xe generation was 0.65 wt%. Measurements are shown in Fig. 4(c). In the central region there is a significant reduction in measured gas that coincided with a marked depletion of Xe around the grain boundaries [9]. These depleted zones have been seen in UO_2 [9] where they were associated with the formation of intergranular bubbles, but the latter were not seen in the MOX COCA.

Overall, the EPMA results in the literature suggest that in more homogeneous MOX fuel, a larger proportion of the Xe generated is retained in the matrix over much of the pellet radius in a measurable form; in solution or in small bubbles. Only in the central region, where the temperature is highest, is there some lost to boundaries and this is most significant near to the boundaries themselves.

7. EPMA of SBR MOX fuel

7.1. General methodology

All the EPMA work on the M501 fuel was carried out at the ITU using their unique shielded instrument [30] that combines Cameca MS46 spectrometers with the

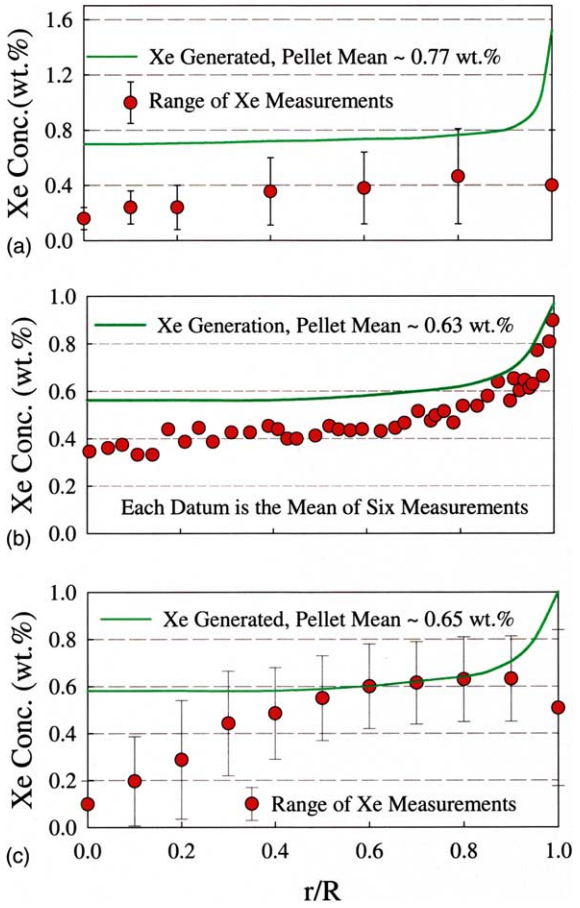

Fig. 4. Radial Xe profiles in (a) MIMAS AUC, (b) OCOM 30 and (c) MOX COCA [9,12]. In each case an integrated pellet mean figure for the generated Xe is given using the equivalence 0.1 wt% Xe ≈ 7.1 MWd/kgHM.

three-lens column of the CAMEBAX probe. The focus of the EPMA investigation was Xe measurement, with particular reference to Pu rich spots. In addition to the determination of the concentration of Xe itself, associated measurements of Cs, Nd, Pu and U are required to evaluate local Xe generation, burnup, and Pu spot characteristics. The measurements may be spot analyses, line scans or concentration profiles obtained from X-ray maps. The EPMA investigation was performed in four stages.

- Pellet matrix radial profiles for Pu, Nd, Xe and Cs to give an overview of fuel performance; Pu loss, burnup (Nd), and Xe generation and retention in the matrix.
- A general survey of Pu spot images across the irradiated pellet to ensure that spots subsequently selected for detailed examination were representative.
- EPMA line scans/maps of individual Pu spots across the pellet in sample CT10 to assess behaviour as a function of radial location/temperature.
- A further comprehensive EPMA examination of the central region of CT20 by imaging and quantitative X-ray mapping of Pu, Nd, Xe and Ru in regions with and without Pu spots.

A voltage of 25 kV was used with beam currents of 100 nA for U and Pu and 250 nA for Nd, Xe and Cs. Xe and Cs were always measured simultaneously, and therefore at exactly the same location, as were U and Pu in a second run. Nd was analysed separately. The uncertainty on measured Cs, Nd and Xe concentrations is 5% relative for concentrations of 0.5 wt%. For Pu concentrations the corresponding figures are 20% relative for concentrations of around 2 wt%, because of overlap with the U spectrum.

Xenon measurement in nuclear fuels is complicated by its precipitation in bubbles. The method adopted here is that devised by Walker [31] and used extensively in the examination of OCOM fuel [12] described later. This method yields the concentration of Xe in solution and trapped in intragranular bubbles smaller than 0.1 μm. At first sight this might seem restrictive. However, the fission gas in fuel is generally to be found in solution, in very small intragranular bubbles, or in large intergranular bubbles that are readily imaged in a SEM. The combination of the two techniques, EPMA and SEM, is therefore sufficient in most cases for tracking Xe distribution.

The FISPIN code [32] was used to determine the quantities of elements present in the M501 fuel after irradiation and cooling to the date of analysis. Nd is a useful indicator of local burnup in the fuel and it was determined that in M501 fuel a measurement of 0.104 wt% Nd would be equivalent to a burnup of 10 MWd/kgHM. Other useful relationships obtained from the code were the following ratios of the various concentrations in wt%.

$$\mathrm{Xe/Nd} = 1.47; \quad \mathrm{Cs/Nd} = 0.89; \quad \mathrm{Xe/Cs} = 1.64.$$

At temperatures below 1200 °C, when it is immobile, Cs provides a reliable indicator of the Xe generation profile in the MOX matrix because of its simultaneous measurement. Neodymium is analysed separately but has been used here to estimate local burnup and Xe generation in and around Pu spots where it is unclear whether Cs has remained immobile.

7.2. Radial concentration profiles and line scans

Pellet radial profiles were obtained by point analysis within matrix grains at intervals of 50–150 μm. The radial profile of Xe generated in the MOX matrix was determined from the accompanying Cs profile, gamma

scanning having confirmed that no significant Cs migration had occurred. U and Pu concentrations were obtained from the average of four peak and three background determinations and Nd, Xe and Cs from the average of six and four. For line scans the electron beam was traversed along a line up to 400 μm long at a scan speed of 8 μm/min. A voltage of 25 kV was maintained with a 100 nA beam current.

7.3. Quantitative X-ray mapping

The technique for the quantitative X-ray mapping of Pu spots and the area surrounding them was developed specifically for the characterisation of SBR MOX fuel. For each spot examined false colour quantitative maps for Nd and Xe were produced, and for some Pu and Ru (indicator for 'Five-metal' fission product inclusions) as well. The beam acceleration voltage and current were the same as those used for line scanning and for radial profiling. The quantitative images were produced at a magnification of 1200× with a resolution of 256 × 256 pixels, giving a pixel size of 0.33 μm. The dwell time per pixel was 350 ms. Quantitative mapping of Pu spots and their surroundings was preceded by the acquisition of an absorbed electron image (AEI), which allowed the influence of gas generated in the spots on the grain boundary bubble distribution in the MOX matrix to be assessed.

Quantitative mapping requires the use of standards and the application of background and matrix corrections to the measured X-ray count in each picture element (pixel). These corrections were made with the Himax® software package and the Xmas® matrix correction both marketed by SAMx. In the resulting X-ray maps, variations in composition are displayed as a range of grey levels, where each pixel has its own quantitative signature. False colour maps were derived from the grey level images using the AnalySIS® image processing software. Quantitative line scans for Nd and Xe were obtained from the maps directly by extracting a line of pixels using a subroutine in the AnalySIS® software package.

Whilst the methodology described above was that used in the SBR MOX examinations, similar procedures, with the exclusion of quantitative X-ray mapping, have been used in the past for the work on OCOM MOX [12] that was reviewed in the previous section. It is also likely that similar techniques were employed in the examinations of the MIMAS AUC reported in [9] which are also discussed below.

8. EPMA results for SBR MOX fuel

8.1. Pellet radial concentration profiles

Fig. 5 shows the distribution of plutonium across the pellet in CT12. As expected there is a reduction in Pu content of the matrix across the irradiated pellet compared with the as-fabricated value ≃4.9 wt%, although the Pu spot distributions and volume fractions remain essentially unaltered [4]. The peak in Pu at the pellet rim arises from the generation of ^{239}Pu through neutron absorption in ^{238}U. The radial burnup profile, calculated from the Nd radial measurements, is also shown in Fig. 5. This also peaks at the pellet rim because of the accumulation of ^{239}Pu.

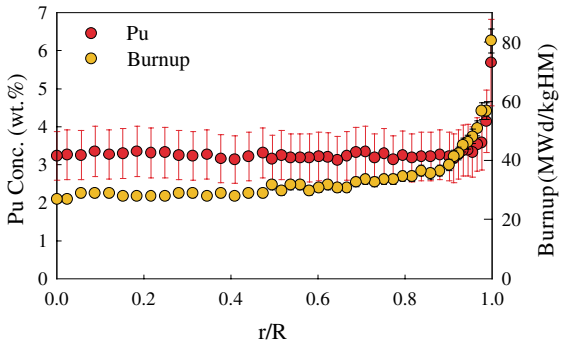

Fig. 5. CT12 radial profile for Pu in the MOX matrix and the burnup calculated from measured Nd using the equivalence 0.104 wt% Nd ≈ 10 MWd/kgHM. The Pu profile is quite uniform and shows a ~45% reduction compared with the as-manufactured enrichment of ~4.9 wt% in the region between the pellet centre and $r/r_0 = 0.8$.

Fig. 6 compares the measured Xe profile with that for generated Xe, calculated from Cs measurements made simultaneously. There is a very good match between the

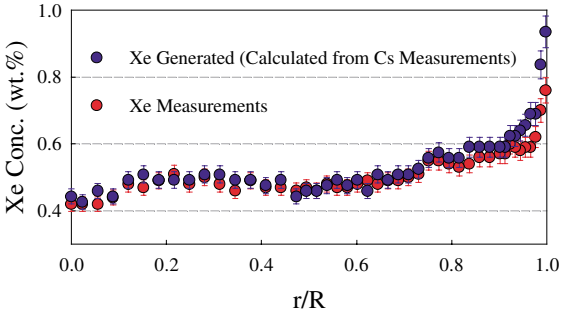

Fig. 6. CT12 radial profile for measured Xe in the MOX matrix compared with Xe generated calculated from Cs measurement. Each Xe and Cs measurement was the mean of six peak and four background determinations. Compared with the measurements made on other MOX fuels, almost all the Xe generated is measured. Over most of the SBR MOX fuel matrix Xe is therefore in solution or in nanometre-sized intragranular bubbles measurable by EPMA. There is some evidence of Xe and Cs migration to the grain boundaries in the fuel centre, and some loss of Xe at the fuel periphery, which is discussed in the text.

two profiles right across the pellet with a hint of Xe loss at the centre and rim. The loss at the periphery is probably due to the formation of relatively large intragranular bubbles in the high burnup rim region; in the centre there is some migration of both Xe and Cs to grain boundaries.

Comparison of Figs. 4 and 6 emphasises the relative homogeneity of SBR MOX. The Xe X-ray maps obtained in CT10 and CT20 confirm this picture of uniformity and provide information on Xe depletion in the pellet centres.

8.2. Appearance of Pu spots across the pellet

The relatively small size of the Pu spots in SBR MOX makes them quite difficult to discern in the irradiated matrix, even towards the outside of the pellet where they can be identified by their high burnup structure (greatly reduced grain size and a high density of gas bubbles). To ensure that representative images were obtained in optical microscopy, a montage was created of micrographs taken across a 400 μm wide radial strip of sample CT11. The careful examination of this led to the selection of the representative images shown in Fig. 7. These show that in the irradiated material, as in the as-fabricated, a proportion of the Pu spots have an associated large (5–10 μm) pore. Study of the montage revealed that ≃55% of Pu spots had such a feature, not significantly different from the proportion in the unirradiated material. This large pore is a consequence of the different diffusion rates of U and Pu atoms during sintering in the manufacturing process. Over the outer two-thirds of the radius the fission gas bubbles generated in the spot are mostly confined to the spot itself or just outside its original perimeter. Only in the central third of the pellet are the bubbles dispersed over a larger volume.

SEM examination of CT10 revealed similar images to the CT11 opticals over most of the pellet radius, as seen from Fig. 7. In the central region 'patches' of intragranular bubbles are seen which are assumed to be related to the proximity of Pu spots, although associated large pores are not always seen. In this region grain boundary bubbles are observed.

8.3. EPMA of Pu spots across the pellet in CT10

Representative images of Pu rich spots at the pellet rim, mid-radius and centre were selected from Pu maps for a detailed study which included false colour X-ray distribution maps for Xe and Nd and extracted concentration profiles across the spots. The data obtained for the spots at the rim and mid-radius were very similar, the main contrast being between these data and the information from a centre spot. Fig. 8(a)–(c) shows the AEI from a mid-radius spot, together with its accompanying false colour X-ray distribution maps for Xe and Nd. Fig. 9(a)–(c) shows the corresponding information from a centre spot, which had no associated as-fabricated pore.

The key features to be extracted from these figures are as follows.

- The average Nd concentrations for the mid-radius and centre spots are ≃1.25 and 1.5 wt%, respectively,

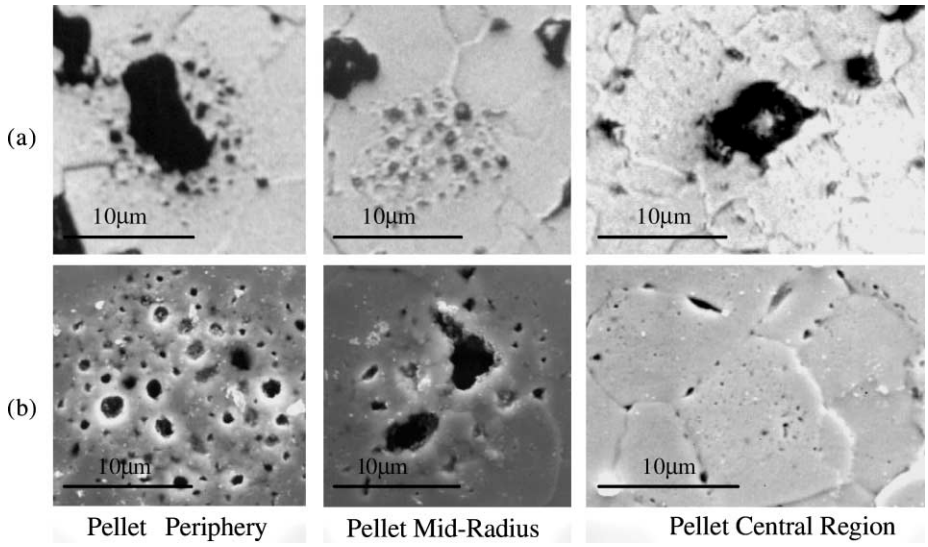

Fig. 7. The appearance of Pu rich spots at the periphery, mid-radius, and centre of pellets of irradiated SBR MOX: (a) CT11 optical micrographs and (b) CT10 SEM. The appearance of the spots does not change significantly over the outer two-thirds of the radius. In the central region the fission gas bubbles are smaller and spread over a larger volume.

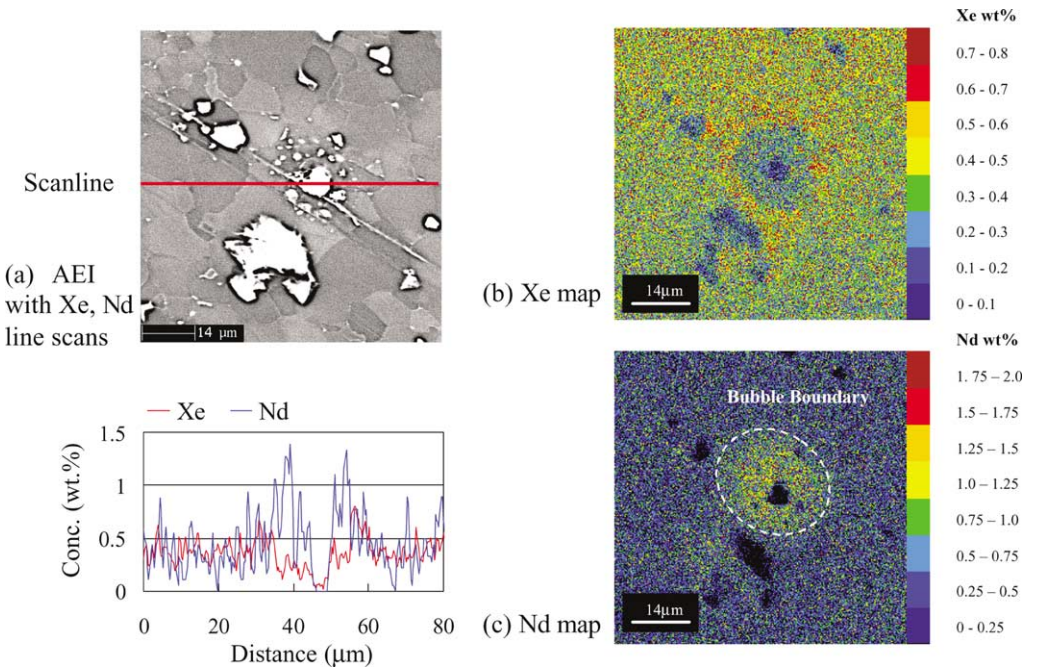

Fig. 8. (a) AEI and quantitative X-ray line scans for Nd and Xe across a Pu spot at the mid-radius of CT10 with corresponding quantitative Xe and Nd X-ray maps. Xe is significantly enriched (a, b) at the periphery of the spot, within the boundary of the Nd rich area in (c). The fission gas bubbles are located within this area.

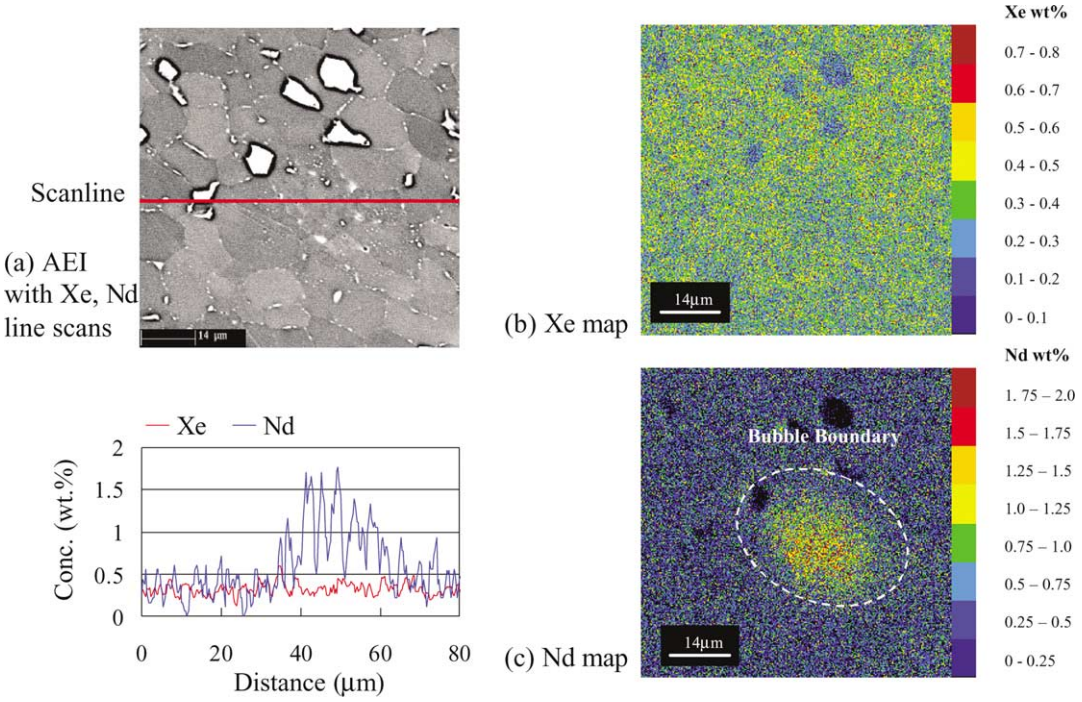

Fig. 9. (a) AEI and quantitative X-ray line scans for Nd and Xe across a Pu spot in the central region of CT10 with corresponding quantitative Xe and Nd X-ray maps. There is a well developed intergranular bubble network and intragranular bubbles exist within the grains surrounding the Pu spot but none within the spot itself. The bubble boundary lies well outside the area where Nd is concentrated indicating that Xe diffusion occurred in addition to recoil. The quantitative X-ray map for Xe appears relatively uniform but close inspection suggests that 'hot spots' exist near the intragranular bubbles.

which indicate local burnups of 120 and 144 MWd/kgHM.

- The Nd figures suggest Xe generation levels of ≃1.84 and 2.2 wt%. Since the measured values are ≃0.3 and ≃0.4 wt% it follows that 80% of the Xe created in each spot has either left the spot or evolved into a form in which it is not measured by EPMA, i.e. bubbles.
- The mid-radius spot has a well-defined region of Xe enhancement ≃0.6 wt% at the outside of the spot, corresponding approximately to the periphery of the Nd distribution. There are also bubbles (>1 μm) spread throughout the area defined by the enhanced Nd distribution. In contrast, the centre Pu spot has no discernible Xe enhancement but a ring of finer-scale (<0.5 μm) bubbles that extends well beyond the limit of the enhanced Nd distribution and into the centre of the neighbouring grains.
- There is a well-defined network of intergranular bubbles in the AEI image of the area surrounding the centre spot. Even in the mid-radius image there are a few boundary bubbles, but there were none at the rim.
- Associated with the appearance of intergranular bubbles in the centre spot image is the apparent depletion of Xe around some boundaries. There is no sign of this in the images from the other pellet locations.

Some of these features, for example the high burnup and bubble formation seen within the rim and mid-radius Pu spots, are similar to those observed in the OCOM and MIMAS fuels. However, the behaviour at the centre, where ≃80% of the Xe generated in the spot is ejected, is quite different. Taken together with the data from the Xe radial concentration profiles the observations indicate the following behaviour.

At the mid-radius, about 0.5 wt% Xe was generated uniformly throughout 99 vol.% of the fuel, over the course of the irradiation. Virtually all this gas was retained in the matrix at this position in the pellet. At the Pu rich spot Xe was generated at a much higher rate consistent with the fissile atom concentration. Approximately 80% of the gas generated in the spot either formed into >1 μm bubbles within the confines of the Pu spot and the recoil range of its fission products, or coalesced into very small intragranular bubbles outside the perimeter of the spot where they were detected by EPMA.

At the pellet centre the radial concentration profiles show that 0.44 wt% Xe was generated uniformly throughout the matrix and that a few percent of this may have been lost to the grain faces where boundary bubbles formed. There is some indication of further loss of Xe from regions immediately adjacent to the boundaries.

At the central Pu spot, ≃80% of the Xe generated was unaccounted for by EPMA measurement. In contrast to observations at the mid-radius position, however, no large >1 μm bubbles were detected within the spot itself but a ring of finer-scale bubbles extended out well into the neighbouring grains. These intragranular bubbles are direct visual evidence of the fate of most of the Xe generated in the Pu spot.

In order to reinforce these observations, further examinations of the central region of irradiated fuel were performed with particular emphasis on (a) the observation of intergranular bubbles, (b) the near grain boundary depletion of Xe, and (c) the formation of intragranular bubbles by gas from Pu spots. Three locations centred around 10 μm Pu spots were examined and compared with two regions free of such spots.

8.4. EPMA of central regions of CT20 with and without ⩾10 μm Pu spots

The examinations of the three regions containing Pu spots around 10 μm in size, gave very similar results, as did two without such spots. Typical examples of each region are shown in Figs. 10 and 11. In addition to the data previously given for the regions of sample CT10 studied by EPMA, Pu maps are presented in both figures and a Ru map in Fig. 10(e).

Key features of these figures are as follows:

- Both regions show extensive grain boundary bubble formation. In each case the variability of the phenomenon is immediately obvious, with, in some instances, adjacent grains displaying widely different levels of swelling. This variability does not appear to be necessarily associated with Pu spots.
- The Pu maps from both regions show a background of 2–5 μm diameter Pu enrichments within the matrix. Typically these areas have Pu concentrations of 6–8 wt%. Despite the presence of these minor perturbations in the Pu concentration the Nd distribution appears uniform.
- Both regions display uniform Xe distribution maps with well defined ≃2 μm depleted zones around boundaries, similar to those seen in MOX COCA and UO_2 [9]. These zones are continuous, extending along regions of boundaries devoid of bubbles, confirming their origin as loss of 'measurable' Xe through diffusion to the boundary rather than artefacts arising from deficient X-ray emission from the intergranular bubbles.
- All three regions with Pu spots show evidence of at least a partial annulus of intragranular bubbles around the spots as seen around the central Pu spot of sample CT10 (see Fig. 9).

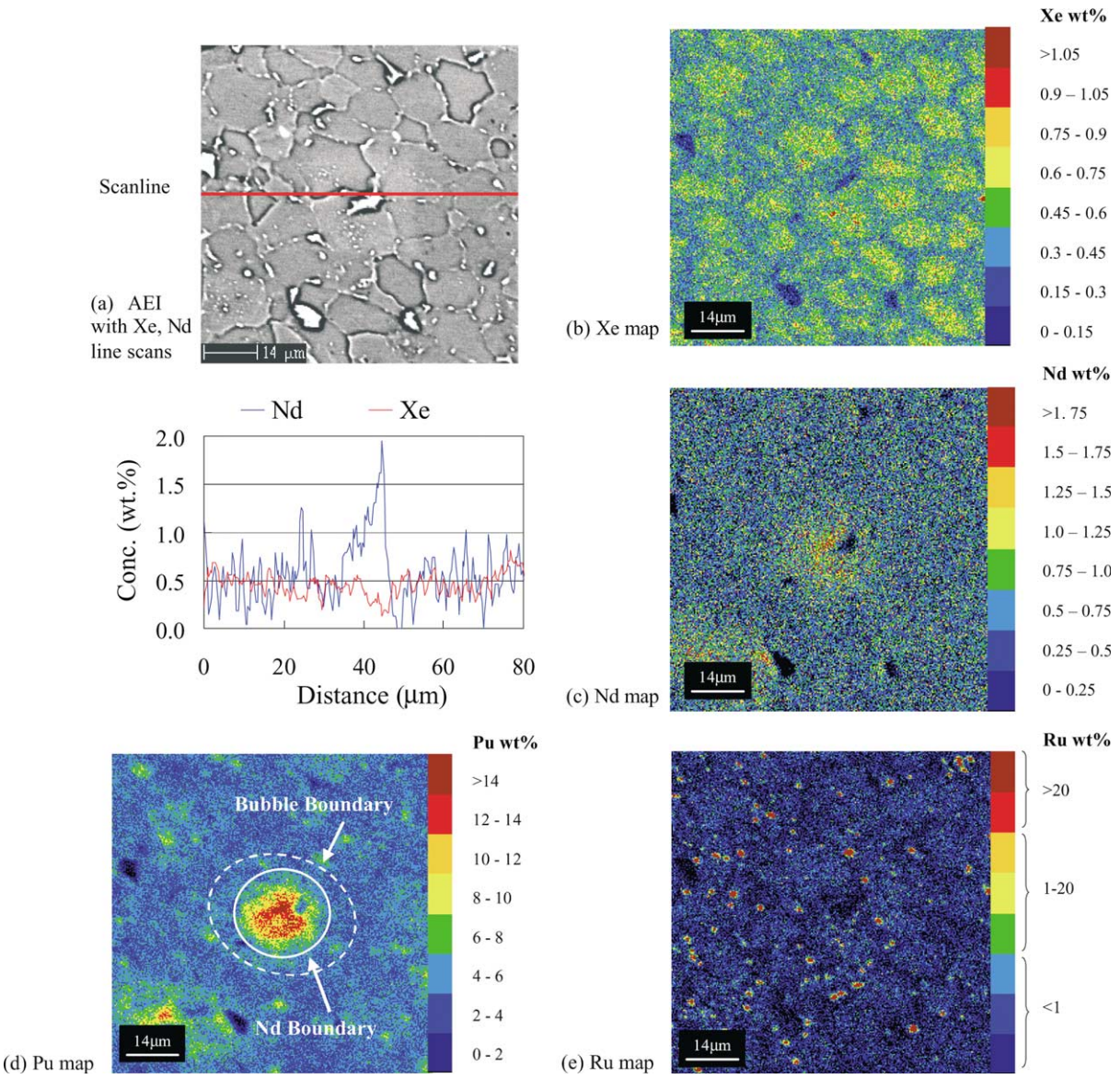

Fig. 10. (a) AEI and quantitative X-ray line scans for Nd and Xe across Pu spot 3 (see Fig. 12) in the central region of CT20. The image actually contains two ~10 μm sized spots as can be seen from the accompanying quantitative Pu and Nd X-ray maps, (c, d), even so, the resultant disruption to the Xe distribution in (b) is minimal. Outside the spot the Xe level is quite uniform as in Fig. 9. (b, c) Quantitative X-ray maps for Xe and Nd corresponding to the image in (a). The presence of a second Pu spot is indicated in the Nd map. The Xe distribution shows marked depletion around grain boundaries although its overall spread is remarkably uniform despite the presence of the Pu spots. (d, e) Quantitative Pu and Ru X-ray maps corresponding to the image in (a). The presence of an additional ~10 μm spot is obvious in the Pu map, and there is a background of smaller spots with low enrichment. Approximate boundaries of bubble and Nd distributions are indicated in (d) for the central spot confirming that significant diffusion of fission gas has occurred in addition to recoil. The Ru map shows the correspondence between 'Five metal' fission product precipitates and grain boundary bubbles previously seen in UO_2 and Callisto-irradiated SBR MOX.

- The average Nd concentration in these regions is ≃1.25 wt% with Xe ≃0.5 wt%, indicating that 75% of the Xe generated in the spots was ejected into the neighbouring grains or perhaps 'lost' in the pores associated with the Pu spots. This figure is slightly lower than the 80% estimated from the CT10 examination.
- The Ru X-ray map in Fig. 10(e) reveals the presence of 'five-metal' precipitates associated with grain

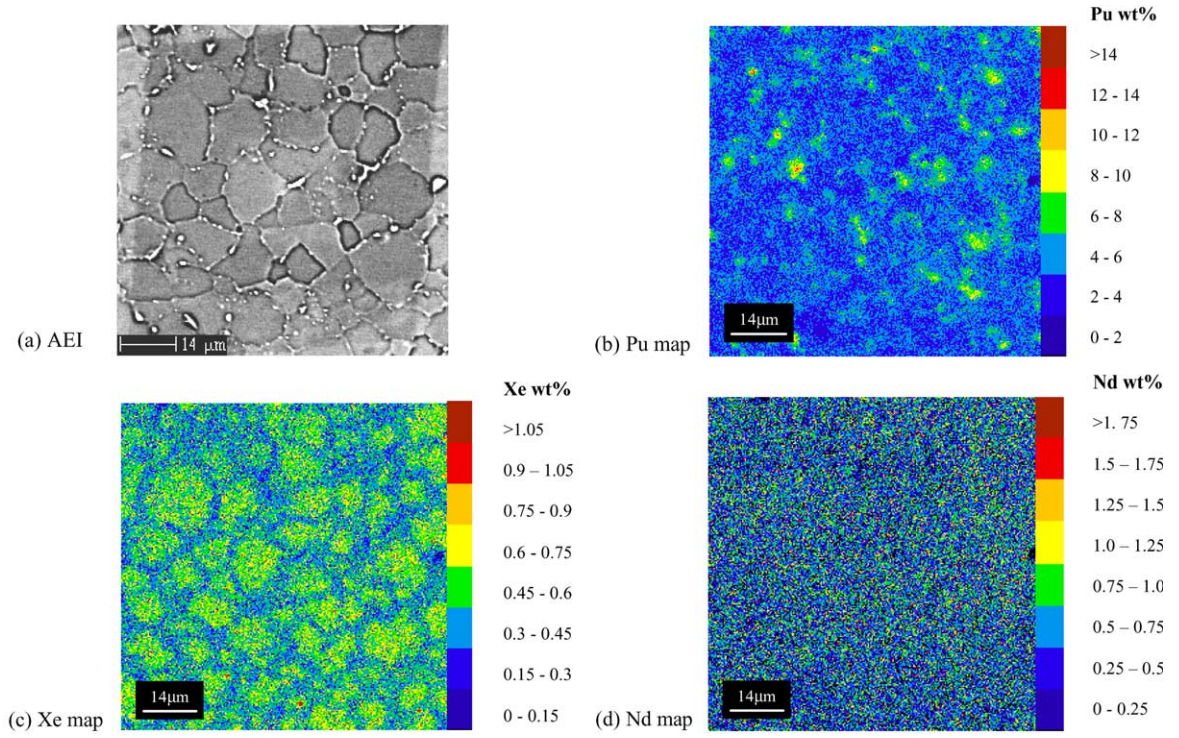

Fig. 11. (a, b) AEI and associated quantitative Pu X-ray map for an area free of ~10 μm Pu spots in the central region of CT20. The Pu map confirms the presence of a relatively uniform dispersion of small, ~5 μm, Pu rich areas with enrichments to 6–8%. These areas have no obvious effect on the Xe distribution in (c) or on the grain boundary bubble network in (a). (c, d) Quantitative Xe and Nd X-ray maps corresponding to the image in (a) showing uniformity of fission product distributions, except for the Xe depletions adjacent to grain boundaries.

boundary bubbles. This is a common feature in UO_2 [15] and was also seen in the SBR MOX fuel irradiated in the Callisto experiment [28] (see Fig. 2(b)).

Fig. 12 shows detailed Xe maps from all three regions with Pu spots studied in CT20. It confirms the presence of a pattern of Xe 'hot spots' in the grains adjacent to the Pu spots, the latter being identified in the images by their associated pores. The concentrations of Xe in these enriched spots reaches at least 0.9 wt% and cannot arise from the observed bubbles since these are too large for their contents to register in EPMA measurement. The 'hot spots' must therefore represent high concentrations of Xe in solution and in nanometre-sized bubbles.

The CT20 investigations therefore confirmed the observations made on sample CT10. They show that the central regions of the SBR MOX fuel rod 4567 contain well-developed networks of intergranular bubbles which appear largely unaffected by the presence of Pu spots. All other aspects of the microstructure seen, such as depletion of Xe near boundaries and Ru precipitation within intergranular bubbles, are also commonly observed in UO_2 [9,15]. The SBR MOX microstructure therefore develops, at least qualitatively, in a similar way as in IDR-UO_2.

9. Xe accountancy

In this section a more quantitative comparison with UO_2 is attempted using measurements made on the intergranular bubbles and Xe X-ray maps. First, an estimate of the degree of inhomogeneity of Xe production in the SBR MOX structure establishes that any resultant variability in grain boundary swelling is well within the range observed in UO_2 fuel. An approximate calculation of the percentage of Xe generated in the matrix that is lost to boundaries is then performed using line scan measurements of Xe that provide the matrix and depleted zone concentrations. The amount of grain boundary swelling in the centre of sample CT10, estimated from SEM micrographs, is then used in conjunction with library images of UO_2 grain faces with similar swelling and known levels of local release to es-

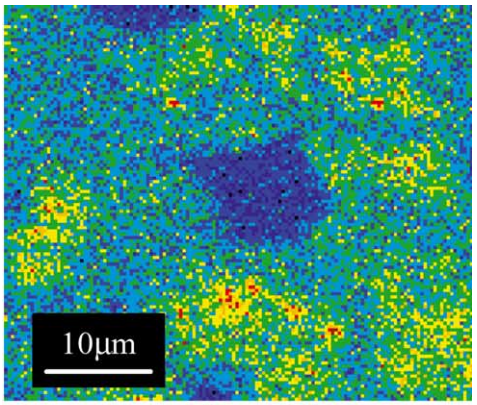

(a) Pu spot 1

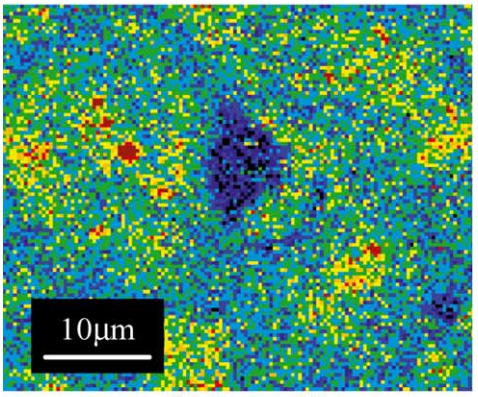

(b) Pu spot 2

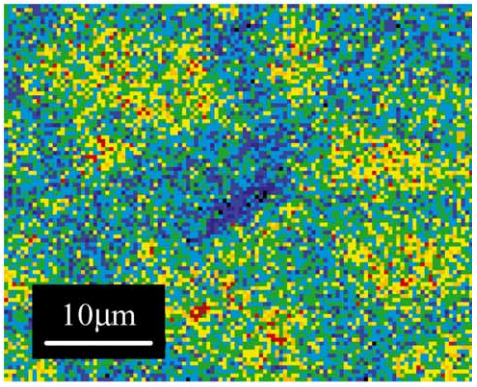

(c) Pu spot 3

Fig. 12. Enlarged Xe X-ray maps of the adjacent grains around all three Pu spots, identified by their associated pores, studied in CT20. All three maps show regions of enhanced Xe concentration in the adjacent grains (red pixels) which are close to the observed encircling annulus of intragranular bubbles (see Fig. 10(d)).

timate the corresponding value for rod 4567. Finally, the above data are compared with the results of the Enigma modelling of rod 4567.

9.1. Inhomogeneity of Xe production in SBR MOX fuel

The degree of inhomogeneity of Xe generation in SBR MOX arising from the presence of fine scale Pu spots was estimated using a simple model based on the microstructural observations. A Pu spot is assumed to replace an average 10 μm matrix grain and, for convenience, to have the same shape, that of the tetrakaidekahedron. This geometrical figure has 14 faces, six square and eight hexagonal, and 36 edges [33]. The volume fraction of Pu spots is assumed to be 1%.

According with the findings in the previous section, each Pu spot in the central region is assumed to generate 4 Xe_G xenon atoms during the irradiation, where Xe_G is the number of xenon atoms uniformly generated within each matrix grain isolated from a Pu spot. Xe_G xenon atoms are assumed to remain in the Pu spot and 3 Xe_G ejected into the neighbouring matrix grains. Each of the 14 grains immediately adjacent to a Pu spot is therefore assumed to contain an additional 3 Xe_G/14 Xe atoms over the number generated locally.

In a matrix grain, under normal circumstances Xe_G/14 Xe atoms are generated per grain face such that for each grain boundary $Xe_G/7 = Xe_B$ atoms are generated, since each boundary is made up of two adjoining grain faces. Of the 196 faces of the 14 grains immediately adjacent to a Pu spot, 72 form boundaries with the other grains bounding the Pu spot. For the 36 boundaries formed by these 72 grain faces the extra Xe present per boundary is $2 \times 3Xe_G/(14 \times 14) = 3Xe_G/98$. This corresponds to 0.21 of the normal generation rate per boundary, Xe_B, so that for these 36 boundaries the generation rate is 1.21 Xe_B. The remaining 124 faces form boundaries with the faces of grains that are not contiguous with the Pu spot. The Xe content of these boundaries is $(Xe_B + 3Xe_G/(14 \times 14)) = 1.11\ Xe_B$.

In a hypothetical cluster of 100 grains containing a single Pu spot there will be 700 grain boundaries, of which 540 are associated with a 'normal' Xe generation of Xe_B atoms per boundary, 36 with 1.21 Xe_B atoms per boundary and 124 with 1.11 Xe_B atoms per boundary. Thus approximately 77% of boundaries have a Xe generation per boundary that is 3% less than if the fuel were completely homogeneous, 5% of boundaries have a Xe generation that is 17% more, and 18% of boundaries that is 8% more. Note that in the absence of Pu spots, normal Xe generation would be 1.03 Xe_B per boundary.

The key question concerning these findings is whether the calculated inhomogeneity in fission gas production would be expected to significantly influence the processes of grain boundary bubble nucleation, swelling, interlinkage and release. The evidence accumulated from UO_2 [16,17] suggests not. As seen from Fig. 2(a) the degree of variability in bubble population seen between grain faces on UO_2 fracture samples can be appreciable.

As pointed out in Subsection 5.5 variations of a factor of ten for number of bubbles on boundaries, and factors of two for individual grain boundary swelling and fractional boundary coverage are commonly observed. It is judged that the estimated additional variability induced by the presence of Pu spots in SBR MOX would be lost within these factors, and this is borne out by the visual evidence.

9.2. Xenon diffusion to boundaries in rod 4567

In order to estimate the percentage of Xe generated lost to boundaries the following procedure was adopted. Five separate line scans from the centre of one grain to the centre of an adjacent grain and perpendicular to the grain boundary were first constructed from the data in the Xe map in Fig. 11(c). From these scans five average figures for the matrix and corresponding depleted layer Xe concentrations were obtained. An estimate of the width of the depleted layer was also obtained from the Xe map in Fig. 11(c) by direct measurement using boundaries that were not overly decorated with bubbles or pores. The loss of Xe was calculated assuming that the loss in the bulk of the grains was negligible, a fact confirmed by radial point analyses for Cs and Xe in CT20. Grains were assumed to be spherical, the lost Xe being calculated from the difference in the matrix and depleted concentrations evaluated over the volume of the depleted shell. Matrix concentrations from the five scans ranged from 0.5–0.6 wt% Xe with corresponding depleted layer figures of 0.36–0.45 wt%. The average depleted zone width, including the layers each side of every boundary, was estimated to be 2 μm. The results in terms of percentage Xe lost to boundaries were surprisingly consistent for the five line scans, varying from 12–15% of the total created. This should be considered an upper limit to the actual amount because of the effects of the grain boundary bubbles themselves on the Xe measurement in the depleted zones.

9.3. Estimation of grain face swelling and local gas release in rod 4567

All of the recent microscopy on UO_2 in the UK [15,17] has been carried out on annealed material using fresh fracture samples that reveal the grain faces. This type of examination has not yet been performed on fuel from rod 4567, but SEM micrographs of transverse polished sections are available. Fig. 13(a) is an example from the centre of section CT10 that clearly shows the presence of grain boundary bubbles. The grain face swelling in sample CT10 was calculated from the image in Fig. 13(a) and then compared with UO_2 samples with similar swelling and known gas release selected from the library of images accumulated during recent post irradiation annealing studies [17].

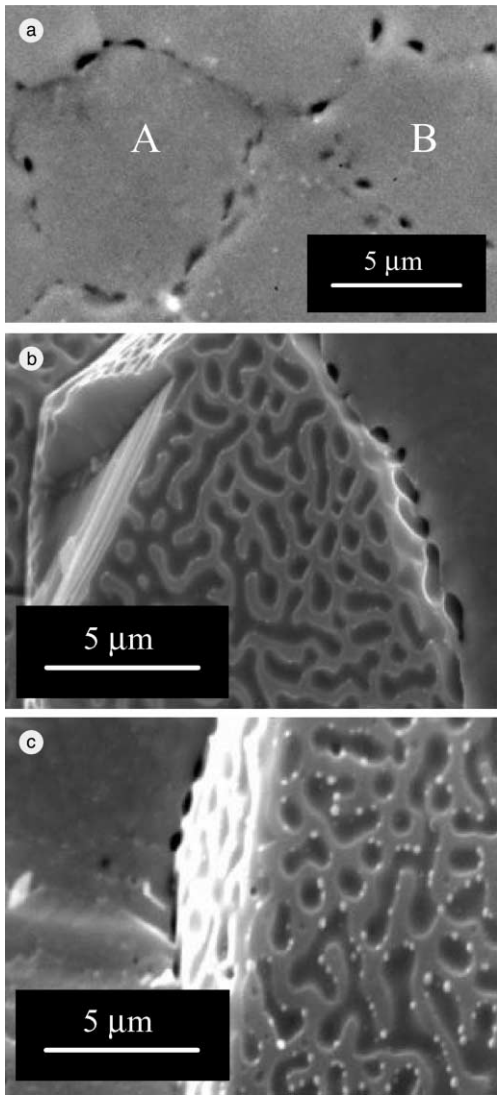

Fig. 13. SEM images of intergranular bubbles in (a) SBR MOX CT10 transverse polished section, (b) grain face in an AGR UO_2 sample which released 5.4% of the fission gas inventory during annealing at 0.5 °C/s to 1900 °C, (c) grain face in an AGR UO_2 sample which released 7.4% of the fission gas inventory during annealing at 20 °C/s to 1700 °C. The three images all show grain face swelling in the range 0.6–1.2%. The burnup of the UO_2 samples is 21 MWd/kgHM.

For the calculation the usual assumptions were made in that the average grain diameter is taken to be 1.5 d_{MLI}, where d_{MLI} is the mean-linear intercept grain diameter, and the average grain face diameter is taken to be 0.56 d_{av} in accordance with the toroid model of [33]. It was further assumed that the length of the grain edges on the transverse section correspond to a chord length of $2/\pi$ times the grain face diameter. The features decorating

the edges are taken to be sections of lenticular bubbles with a projected radius of R_p on the grain face and therefore a length of $2R_p$.

The volumetric swelling, $\frac{\Delta V}{V}$, was calculated using Eq. (1) from Ref. [34],

$$\frac{\Delta V}{V} = \frac{3}{d_{av}} D_B \frac{4\pi}{3} R_p^3 \frac{\left(1 - \frac{3\cos\theta}{2} + \frac{\cos^3\theta}{2}\right)}{\sin^3\theta}, \quad (1)$$

where d_{av} is the average grain diameter, D_B is the gas bubble density per unit area on the grain face, R_p is the mean bubble radius and θ is the dihedral angle for a lenticular gas bubble, which, from measurements in UO_2 is 50°. The term $3/d_{av}$ is the conversion factor for translating swelling per unit area of grain boundary to swelling per unit volume of fuel and, D_B is given by

$$D_B = \frac{N_B}{N_C C_L 2R_p}, \quad (2)$$

where N_B is the number of bubbles on the grain edges, N_C is the number of chords corresponding to the number of grain edges appearing in the transverse cut through the grain and C_L is the mean chord length. The measured values of N_B, N_C, C_L and R_p for grains A and B in Fig. 13(a) are listed in Table 5 and when inserted in Eq. (2) give bubble densities per μm^2 of 1.45 and 0.98, respectively. It can be seen from Fig. 2 in Ref. [17] that in ramp tested and annealed UO_2 these densities correspond to an average bubble area per boundary of 0.3–0.4 μm^2 which equates to a mean bubble radius, R_p, of 0.3–0.35 μm. The later size range is remarkably similar to the mean bubble radius measured on the boundaries of grains A and B shown in Fig. 13(a). When the above values of D_B together with the grain diameter, d_{av}, calculated from the mean grain boundary length and grain face diameter are inserted into Eq. (1), grain face swelling values of 1.06% and 1.21% are obtained for grains A and B as shown in Table 5. These two grains selected for measurement were amongst the most decorated in the sample so the calculated levels of swelling may be regarded as a upper limit for the CT10 sample.

Table 5
Data from intergranular bubble measurements on the two grains in CT10 identified in Fig. 13(a) and the calculated volumetric swelling

Grain	No. of chords	Mean chord length (μm)	No. of bubbles	Mean bubble radius, R_p (μm)	Swelling (%)
A	5	5.7	24	0.29	1.06
B	6	4.9	19	0.33	1.21

Fig. 13(b) and (c) shows two UO_2 grain faces with swellings of 0.9% and 0.6%, respectively, slightly less than that estimated for grains A and B in sample CT10. These images from post-irradiation annealed UO_2 specimens were selected not only because of the degree of swelling, but also because in each case the particular geometry of the grain allows a 'transverse' view of the adjacent grain face and this is seen to have an appearance matching the CT10 boundaries. The measured local gas releases for these UO_2 samples were 5.4% and 7.4%, respectively. It is therefore judged that the grain boundary decoration seen in Fig. 13(a) is consistent with a local release of similar magnitude.

9.4. Comparison of estimates for Xe loss from grains and local gas release to the rod free volume with Enigma calculations

The Enigma calculations referred to in this section are part of the output from the modelling performed in [5]. This was carried out with a version of the code that is UO_2 based but with values of thermal conductivity and grain size appropriate to SBR MOX. The release calculated for rod 4567 was 1.0% [5], in good agreement with the measured figure of 1.1%. The Enigma output for this run also included figures for grain growth, the fraction of generated fission gas diffused to boundaries, and local release within radial zones in the rod as a function of axial position.

The two rod sections used for the EPMA/intergranular bubbles studies, CT10 and CT20, had similar ratings and burnups (see Table 3). Therefore, only the relevant data for the axial position of CT20 was extracted from the ENIGMA output. Area average values for the fractions of gas remaining in the grains and on grain boundaries were obtained for the inner third of the fuel at this location. The results obtained translate into figures of 13% for the gas diffused to boundaries with 9% local gas release to the rod free volume. The measured or estimated data for these quantities are consistent with these numbers.

10. Post-irradiation annealing of UO_2 and SBR MOX compared

Thus far, the similarity between fission gas behaviour in SBR MOX and UO_2 fuel has been inferred from a comparison of the observations and measurements of the Xe distribution and associated intergranular bubble network in SBR MOX with the data reported [9] for PWR-irradiated UO_2, SEM images from annealed AGR fuel and calculations made with the Enigma code. In order to provide a direct comparison in which the effects

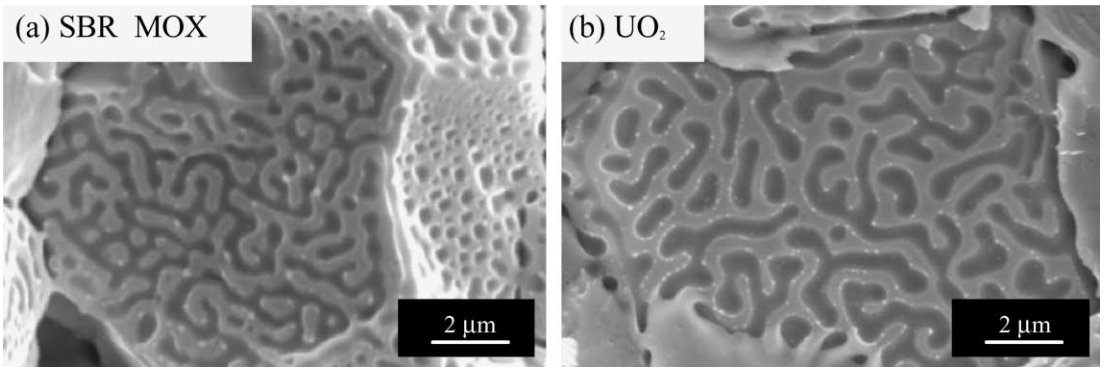

Fig. 14. SEM images of grain faces decorated with gas bubbles after post irradiation annealing: (a) SBR MOX fuel and (b) AGR UO_2 fuel. The MOX fuel was one-cycle fuel commercially irradiated to 11.5 MWd/kgHM and the UO_2 fuel had been irradiated in the Halden Reactor to 9 MWd/kgHM. The annealing tests were nominally identical; after conditioning at 1000 °C the fuel was ramped to ~1900 °C at 0.5 °C/s and then quenched. At the final temperature reached in the MOX fuel, 1876 °C, the gas release was 6.2% and at the same temperature in the UO_2, 4.5%.

of thermal conductivity and fuel rating are eliminated, identical post-irradiation annealing experiments have recently been performed on both fuel types [35]. In these experiments low burn-up, one-cycle, SBR MOX and AGR UO_2 were used to ensure that the two fuels were seeded with gas, but that the development of the microstructure was minimal. The fuel was first conditioned at 1000 °C and then slow ramped at 0.5 °C/s to about 1900 °C. This rate was chosen because experience with post-irradiation annealing experiments has shown that relatively slow temperature transients tend to result in equilibrium intergranular bubble populations similar to those observed under lower temperature steady-state irradiation conditions. Typical SEM images of the intergranular bubble networks in the SBR MOX fuel and the AGR UO_2 fuel are shown in Fig. 14. The two bubble morphologies show the same general features, although there was a small difference in the measured releases of these annealed fuels at 4.5% (UO_2) and 6.2% (SBR MOX), which could be attributable to the effect of grain size. This single experiment confirms that the processes and parameters associated with gas release in the two fuels are essentially identical and that any differences in in-pile behaviour are attributable to the thermal conductivity, power rating or, at higher exposures, grain size.

11. Summary and conclusions

The microstructure and microchemistry of irradiated SBR MOX fuel have been examined in detail and comparisons made with IDR-UO_2 and other MOX fuel, where suitable data are available. It has been shown that the as-fabricated features which influence release, such as grain size, porosity and dislocation density, are either similar in magnitude in the two fuels or do not significantly influence gas release at the level considered. It has also been demonstrated that the irradiation-induced parameters such as fission gas production rate, fission gas diffusivity, grain growth and intragranular bubble morphology are equivalent in the two fuels.

The most significant feature observed in SBR fuel is a well-developed grain boundary bubble network. Such networks have not been seen previously in other MOX fuels irradiated under normal PWR conditions, although they have been reported in UO_2.

The key sections of the paper are those that describe the characteristics of the Pu spots in commercially irradiated SBR MOX. In several ways their behaviour is similar to that of the Pu spots seen in OCOM and MIMAS MOX fuels. For example, they have a much higher burnup than the surrounding matrix and develop internal fission gas bubbles in the colder outer half of the fuel. However, there are important differences. In SBR MOX fuel the Pu spots are around 10 μm in size and only about 4% of the fission gas is generated within the Pu spot. Moreover, owing to the relatively small size of the Pu spots, in the central region of the pellet where release occurs under normal operations most of the fission gas generated in the Pu spots is deposited within the neighbouring grains, through a combination of recoil and diffusion. In contrast, in other MOX fuels, the majority of the fission gas is generated within the much larger Pu rich inhomogeneities where it is chiefly retained in pores, even in the pellet centre.

In SBR MOX fuel the perturbation in the otherwise uniform generation of Xe within the MOX matrix which is caused by the Pu spots has been shown quantitatively to be well within the natural variability in grain boundary swelling seen in UO_2. Moreover, very detailed

examinations of the grain boundary microstructures in central regions with and without Pu spots reveal no visual evidence of such a perturbation outside the general boundary to boundary variability inherent in intergranular bubble formation.

By comparing it with IDR-UO_2 data, the grain boundary swelling in the highest temperature region of SBR MOX rod 4567, which had an overall release of $\simeq$1.1%, has been shown to be consistent with a local release in the range 5–8%. This requires a higher fraction of gas to have diffused to boundaries, and this was confirmed by EPMA measurements of Xe loss of 12–15% of that generated, most of which has diffused from the zones adjacent to the boundaries in the central regions.

Overall the microstructure and microchemistry of SBR MOX irradiated for three cycles are entirely consistent with its measured fission gas release, and with the mechanisms of release identified in UO_2. Differences in behaviour are attributable to the higher irradiation temperatures reached in the MOX material as a result of its lower thermal conductivity and a generally higher third-cycle rating imposed by operational constraints. When these features are incorporated in a UO_2 based version of the Enigma fuel performance code, together with the appropriate grain size, the predictions for local and overall gas release, and gas diffusion to boundaries, are in good agreement with the figures above.

References

[1] P.M.A. Cook, I.D. Palmer, R. Stratton, C.T. Walker, in: IAEA International Symposium on MOX Fuel Cycle Technologies for Medium and Long-Term Deployment, Vienna, Austria, 1999, Paper no. IAEA-SM-358-16, p. 233.

[2] C. Brown, P.M.A. Cook, J. Edwards, S.B. Fisher, G.A. Gates, I.D. Palmer, R.J. White, in: TopFuel'99, Avignon, France, SFEN, Paris, 1999, p. 223.

[3] P.M.A. Cook, R. Stratton, C.T. Walker, in: ANS International Topical Meeting on LWR Fuel Performance, Park City, Utah, USA, ANS, La Grange Park, Ill., 2000, p. 653.

[4] P. Ivison, P.M.A. Cook, S. Bremier, C.T. Walker, in: IAEA TCM on Nuclear Fuel Behaviour Modelling at High Burnup and its Experimental Support, Windermere, England, 19–23 June 2000, p. 239.

[5] R.J. White, S.B. Fisher, P.M.A. Cook, R. Stratton, C.T. Walker, I.D. Palmer, J. Nucl. Mater. 288 (2001) 43.

[6] R. Weston, I.D. Palmer, J.M. Wright, G.D. Rossiter, R.C. Corcoran, T.C. Gilmour, C.T. Walker, S. Bremier, in: ENS TopFuel 2001, Stockholm, Sweden, 27–30 May 2001, Paper no. P2-9.

[7] I.D. Palmer, R.J. White, G. Rossiter, in: IAEA International Symposium on MOX Fuel Cycle Technologies for Medium and Long-Term Deployment, Vienna, Austria, 1999, Paper no. IAEA-SM-358-20, p. 271.

[8] P. Deramaix, D. Haas, J. van de Velde, Nucl. Technol. 102 (1993) 47.

[9] Y. Guerin, J. Noirot, D. Lespiaux, C. Stuzick, P. Garcia, P. Blanpain, G. Chaigne, in: ANS International Topical Meeting on LWR Fuel Performance, Park City, Utah, USA, ANS, La Grange Park, Ill., 2000, p. 706.

[10] P. Garcia, A. Boulore, Y. Guerin, M. Trotobas, P. Goeriot, in: ANS International Topical Meeting on LWR Fuel Performance, Park City, Utah, USA, ANS, La Grange Park, Ill., 2000, p. 679.

[11] W. Goll, H.P. Fuchs, R. Manzel, F. Schlemmer, Nucl. Technol. 102 (1993) 29.

[12] C.T. Walker, W. Goll, T. Matsumura, J. Nucl. Mater. 228 (1996) 8.

[13] P. Ivison, S.B. Fisher, in: TopFuel'99, Avignon France, 13–15 September 1999, SFEN, Paris, 1999, p. 504.

[14] R.J. White, in: ANS Topical Meeting on LWR Fuel Performance, West Palm Beach, Florida, USA, April 1994, p. 196.

[15] C. Baker, R. Corcoran, A.T. Donaldson, R.J. White, in: Extended Halden Project Group Meeting, Loen, Norway, May 1996, HPR-347, vol. 2, Paper no. 25.

[16] R.J. White, in: IAEA TCM on Nuclear Fuel Behaviour Modelling at High Burnup and its Experimental Support, Windermere, UK, 19–23 June 2000, p. 91.

[17] R.J. White, in: International Seminar on Fission Gas Behaviour in Water Reactor Fuels, Cadarache, France, 26–29 September 2000, NEA/OECD, 2002, p. 189.

[18] M. Edenius, D. Knott, K. Smith, in: Proceedings of the International Conference on the Physics of Nuclear Science and Technology, Long Island, NJ, USA, October 1998, vol. 1, p. 135.

[19] J.A. Turnbull, C.A. Friskney, J.R. Findlay, F.A. Johnson, A.J. Walker, J. Nucl. Mater. 107 (1982) 168.

[20] G. Gates, in: IAEA TCM on Nuclear Fuel Behaviour Modelling at High Burnup and its Experimental Support, Windermere, England, 19–23 June 2000, p. 257.

[21] A.H. Booth, A Method for Calculating Fission Gas Diffusion from UO_2 and its Application to the X-2-f Loop Tests, Report AECL-496, 1957.

[22] Y. Irisa, K. Murai, K. Goto, S. Suzuki, R. Sabate, J.M. Alonso, in: ANS International Topical Meeting on LWR Fuel Performance, Park City, Utah, USA, ANS, La Grange Park, Ill., 2000, p. 471.

[23] K. Goto, S. Matsumoto, T. Murata, T. Miyashita, H. Anada, H. Abe, in: ANS International Topical Meeting on LWR Fuel Performance, Park City, Utah, USA, ANS, La Grange Park, Ill., 2000, p. 457.

[24] S. Abeta, T. Takahashi, S. Doi, in: TopFuel'97, Manchester, UK, 9–11 June 1997, British Nuclear Energy Society, London, p. 2.40.

[25] P.E. Hart, J.L. Daniel, in: International Conference on Ceramic Microstructures, August 1976, Berkeley CA, USA, Westview Press, Boulder, CO, 1976, p. 710.

[26] C. Baker, J. Nucl. Mater. 66 (1977) 283.

[27] J.A. Turnbull, J. Nucl. Mater. 38 (1971) 203.

[28] J. Mullen, C. Brown, I.D. Palmer, P. Morris, in: TopFuel'97, Manchester, UK, 9–11 June 1997, British Nuclear Energy Society, London, p. 4.23.

[29] G.J. Dienes, A.C. Damask, Point Defects in Metals, Gordon and Breach Science, New York, 1963.

[30] C.T. Walker, J. Anal. At. Spectrom. 14 (1997) 447.
[31] C.T. Walker, J. Nucl. Mater. 80 (1979) 190.
[32] R.F. Burstall, FISPIN – A Computer Code for Nuclear Inventory Calculations, BNFL, Sellafield, UK, Report ND-R-328, 1979.
[33] M.O. Tucker, J. Nucl. Mater. 79 (1979) 199.
[34] P.J. Clemm, J.C. Fisher, Acta Met. 3 (1955) 3.
[35] J.S. Punni, M.A. Mignanelli, Post-Irradiation Annealing Tests on SBR MOX Fuel, Report AEAT/R/NS/0418, 2001.